Applied Materials Today 44 (2025) 102723

Contents lists available at ScienceDirect

Applied Materials Today

journal homepage: www.elsevier.com/locate/apmt

Tetrandrine-loaded electrospun scaffold modulates inflammation and fibroblast activity to promote tendon regeneration

Xinyan Chen [a,c,#], Xiao Yu [a,#], Hao Feng [a,#], Panpan Shang [b], Muhammad Shafiq [d], Zhengchao Yuan [a], Cheng Li [e], Zewen Wang [e], Zhenchao Liu [e], Yuan Yao [e], Mohamed EL-Newehy [f], Meera Moydeen Abdulhameed [f], Yan Xiong [g,*], Yuan Xu [e,*], Xiumei Mo [a,b,**]

[a] State Key Laboratory for Modification of Chemical Fibers and Polymer Materials, Shanghai Engineering Research Center of Nano-Biomaterials and Regenerative Medicine, College of Biological Science and Medical Engineering, Donghua University, Shanghai 201620, China
[b] Institute of Biomaterials and Biomedicine, School of Food and Pharmacy, Shanghai Zhongqiao Vocational and Technical University, Shanghai 201514, China
[c] School of Biomedical Sciences and Engineering, Guangzhou International Campus, South China University of Technology, Guangzhou 511442, China
[d] Innovation Center of NanoMedicine (iCONM), Kawasaki Institute of Industrial Promotion, Kawasaki-ku, Kawasaki 210-0821, Japan
[e] Department of Orthopaedics, Xinqiao Hospital, Army Medical University, No.183, Xinqiao Street, Shapingba District, Chongqing 400037, China
[f] Department of Chemistry, College of Science, King Saud University, P.O. Box 2455, Riyadh 11451, Saudi Arabia
[g] Department of Orthopaedics, Daping Hospital, Army Medical University, Chongqing, China

ARTICLE INFO

Keywords:
Electrospinning
Tendon repair
Tetrandrine
Anti-inflammatory
Scaffolds
Knitted scaffolds

ABSTRACT

The effectiveness of tendon regeneration is impeded by an excessive inflammatory response as well as uncontrolled proliferation of fibroblasts. Transplantation of tendon substitutes which can balance inflammatory response while constrict aberrant proliferation of fibroblasts is a key to promote functional tendon regeneration. The objective of this study was to design electrospun tetrandrine-loaded polylactic acid/silk fibroin (PLLA/SF) nanofibers and then fabricate them into knitted scaffolds. Briefly PLLA micron yarns were coated with PLLA/SF nanofibers and processed into knitted scaffolds. The incorporation of tetrandrine into fibers resulted in a significant suppression of fibroblast proliferation ($p < 0.05$) and promoted macrophage polarization into anti-inflammatory phenotypes, with a CD206/CD68 ratio increase of 2.5-fold compared to the control. Additionally, knitted scaffolds delayed the inflammatory response and enhanced collagen production at the repair site *in vivo*. Taken together, our approach of simultaneously harnessing structural and biological cues in the form of an antiproliferative and anti-inflammatory therapeutic alongside PLLA/SF-coated nanoyarns afforded knitted scaffolds. The bifunctional regulation of tetrandrine simultaneously addressing inflammation resolution and fibrotic inhibition represents a strategic advance over existing mono-functional drug-loaded scaffolds.

1. Introduction

Tendons are connective tissues responsible for connecting the muscles to the bones. Tendon tissues are responsible for the conversion of mechanical forces produced by the contraction of the muscle into the movement of the joints [1]. Tendon injuries represent a serious challenge for orthopedic surgeons as these defects often respond slowly to the treatment, thereby necessitating prolonged recovery [2,3]. Current gold-standard treatment modality for the degenerated tendon is surgical operation albeit its marginal effectiveness as well as several post-operative complications, which are generally ascribed to different types of factors, such as inflammatory response and abnormal proliferation of fibroblasts [4–6]. While these factors are necessary for tendon healing, aberrant inflammation and over-proliferation of fibroblasts can lead to numerous abnormalities, such as cell apoptosis, tissue adhesion, and scar tissue formation [7,8]. Moreover, owing to the limited ability of

* Corresponding authors.
** Corresponding author at: State Key Laboratory for Modification of Chemical Fibers and Polymer Materials, Shanghai Engineering Research Center of Nano-Biomaterials and Regenerative Medicine, College of Biological Science and Medical Engineering, Donghua University, Shanghai 201620, China.
E-mail addresses: xiongyandoctor@tmmu.edu.cn (Y. Xiong), 15123161526@163.com (Y. Xu), xmm@dhu.edu.cn (X. Mo).
# Xinyan Chen, Xiao Yu and Hao Feng contributed equally to this work.

https://doi.org/10.1016/j.apmt.2025.102723
Received 17 January 2025; Received in revised form 4 April 2025; Accepted 8 April 2025

the tendon to slide during flexion, there is a high recurrence rate of tendon injuries following repair [9,10]. Consequently, inflammation resolution and well-regulated proliferation of fibroblasts are keys to realize a healthier yet an effective tendon repair.

Electrospun fibers and hydrogels are widely utilized as tendon substitutes [11]. Electrospun fibers possess high surface area-to-volume ratio and therefore they can recapitulate the structural and morphological features of the extracellular matrix (ECM) [12,13]. However, fibers alone may not give a desired effect for tendon repair, thus drugs with anti-inflammatory and anti-fibrosis abilities are needed. Yan et al. [14] fabricated ibuprofen (IBU)-loaded poly(lactic-co-glycolic acid) acid (PLGA)-based fibers; drug loading suppressed the production of inflammatory factors while increased the production of collagen type I alongside sufficient tendon regeneration. Despite the advantageous features of electrospun membranes, they cannot meet the stringent mechanical requirements of the native tendon tissues, *e.g.*, ultimate tensile strength (UTS), 5–100 MPa and Young's modulus: 20–1200 MPa (human patellar tendon) for tendon repair, which are responsible for initiating long-term tendon structure modifications, and effecting the mechanical properties of healed tendons [15–17]. Yu et al. [18] fabricated a double-layer core-spun yarn (DY) with nanofibers conjugated with naproxen sodium (NPS) conjugated to polylactic acid (PLLA) micron fiber yarn by electrospinning. Drug-loaded micron yarns promoted macrophages polarization towards an anti-inflammatory phenotype, thereby resolving the inflammatory response and promoting tendon repair. While these studies emphasized upon the anti-inflammatory ability of scaffolds, an over-proliferation of fibroblasts is also an impediment for the poor healing of the tendon tissues [19]. Therefore, a drug with activities alongside anti-inflammatory characteristics and well-regulated proliferation of fibroblasts is necessitated to improve bioactivities of scaffolds.

Tendon repair is regulated by different types of cytokines and chemokines; these bioactive cues are produced by the cells located at the injury site [20]. Transforming growth factor-beta (TGF-β) is one of those factors. An aberrant TGF-β1 expression as well as altered intracellular signaling are closely related to the remodeling and over-proliferation of fibroblasts, thereby leading to abnormal ECM deposition, fibrosis, and scar tissue formation [21–23]. Tetrandrine is a natural bis benzylisoquinoline alkaloid, which is isolated from the root of Stephania tetrandrian and has been shown to resolve inflammation, suppress ECM deposition, and lessen fibrosis [24] (Fig. 1a). Lin et al. [25] reported tetrandrine-mediated inhibition of TGF-β1 as well as its intracellular signaling via SMAD family member 7 (Smad7) induction and SMAD family member 2 (Smad2) inhibition. Therefore, tetrandrine suppressed the production of Col-I and Col-III. Gao et al. [26] reported tetrandrine-mediated inflammation resolution presumably due to the constricted phosphorylation of nuclear factor kappa-B (NF-κB) p65 and inhibitor of NF-kappa-B alpha (IκBα) in macrophages as well as chondrogenic ATDC5 cells.

Polylactic acid (PLLA) is a biocompatible and a biodegradable polymer with low immunogenicity, non-toxicity, and good mechanical properties. The PLLA can be easily electrospun to produce fibers [27]. Nonetheless, PLLA exhibits poor biocompatibility owing to the lack of cell recognition sites as well as its hydrophobicity, which limit its potential for tissue regeneration [28]. Silk fibroin (SF) is a natural protein with excellent biocompatibility, biodegradability, anti-inflammatory characteristics, and air permeability [29] (Fig.1b). The SF is also conducive for cell adhesion, cell migration, cell proliferation, and cell differentiation [30].

The overarching objective of this study was to fabricate tetrandrine-loaded composite fibers based on PLLA and SF and fabricate knitted scaffold for tendon tissue regeneration. Drug-laden PLLA/SF nanofibers were fabricated using electrospinning and wrapped on the surface of the PLLA micron fiber yarn to afford core-sheath type nanoyarns. The nanofibers can recapitulate ECM microenvironment *in vivo* and may additionally leverage a conducive microenvironment for cell

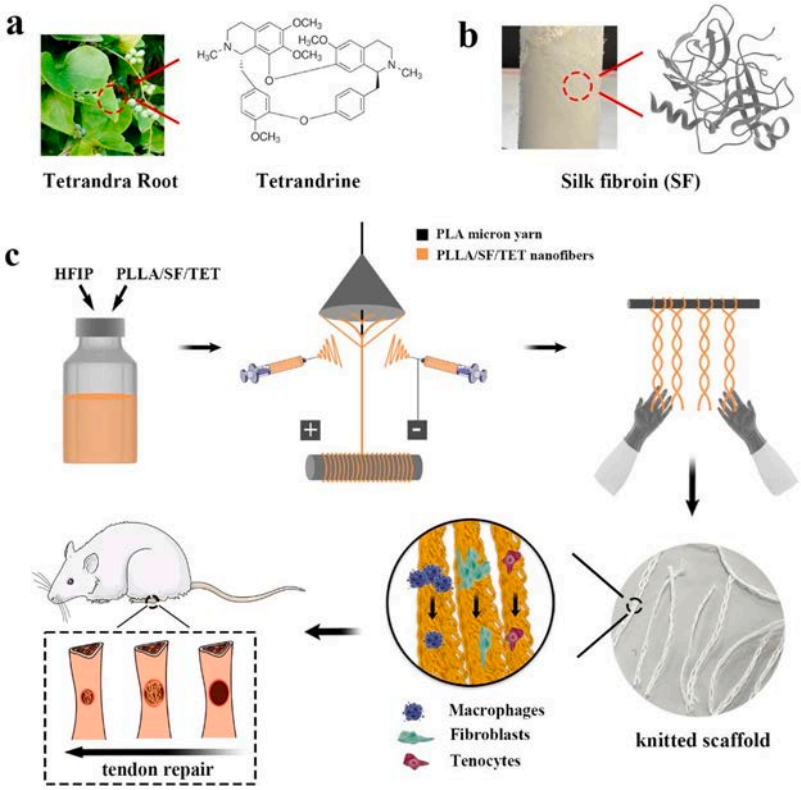

Fig. 1. Schematic illustration of materials and preparation of electrospun fibers and knitted scaffolds. Tetrandrine (Tet) was extracted from tetrandra roots (a). Silk fibroin (SF) was extracted from cocoons (b). PLLA/SF/Tet nanofibers were amassed onto the PLA yarn, then knitted into scaffolds. The scaffolds could adjust the polarization of macrophages, inhibit the proliferation of fibroblasts, and promote tendon repair (c).

proliferation, while PLLA micron fiber yarn can confer good mechanical properties to the scaffolds. The tetrandrine could inhibit inflammation as well as regulate the ration of fibroblasts. Nanoyarns were knitted into scaffolds for improved mechanical properties and stability than that of the single yarns. Due to its abilities of mimicking EMC microenvironment, as well as inhibiting excessive inflammatory response and fibroblasts proliferation, the knitted scaffold is promised to serve as a new tendon substitute with potential to promote tendon repair (Fig. 1c).

2. Experimental

2.1. Materials

The silk cocoons were purchased from Northwest Sericulture Base (Shanxi, China). Polylactic acid (PLLA, Mw = 110 kDa) was bought from Shanghai Yien Chemical Technology Co., Ltd (Shanghai, China). Tetrandrine (analytically pure) was purchased from Shanghai Aladdin Biotechnology Co., Ltd (Shanghai, China). The PLLA micron fiber yarn was purchased from College of Textiles, Dong Hua University (Shanghai, China). The Hexafluoroisopropanol (HFIP, analytically pure) was bought from Shanghai DaRui Chemical Technology Co., Ltd (Shanghai, China). RAW264.7 macrophages and NIH-3T3 fibroblasts were obtained from the Cell Bank of the Chinese Academy of Sciences (Shanghai, China). Tenocytes were extracted from two-week-old SD rats based on previous reports [31,32].

2.2. Extraction of silk fibroin

Silk fibroin (SF) was extracted from cocoons according to a previous report [33]. Briefly, 60 g cocoons were boiled in 0.05 % (w/v) sodium carbonate (Na_2CO_3) three times to remove sericin. Silk without sericin was completely dissolved in 78 % (w/v) lithium bromide (LiBr) solution, filtrated, and dialyzed for up to 5 d to obtain silk protein solution. The solution was frozen at −80 °C overnight and freeze-dried (FreeZone 2.5, Labconco, USA) to afford solid SF for the subsequent use.

2.3. Preparation of electrospun fibers and knitted scaffolds

PLLA/SF (3:1, w/w) were dissolved in HFIP to afford 20 % (w/v) solution. Different contents of tetrandrine (*e.g.*, 2, 4, 8, 16 μg/mL, etc.) were added into PLLA/SF solution and allowed to stir for 10 h at room temperature (r.t.) for homogeneous dispersion. The nanofiber yarns were prepared by a custom-made electrospinning apparatus (TEADFS-700, BeiJing Technova Technology, China). In-house assembled electrospinning setup was comprised of a rotating funnel, two propelling pumps, two syringes, and a collecting roller was employed to fabricate fibers. Two 20 G needles were mounted on the syringes, with a positive and negative high-voltage power of 10 kV applied at each end. The mixed solutions were delivered by the propelling pumps at a flow rate of 1.8 mL/h. The PLLA micron fiber yarn was passed through the rotating funnel, which was rotating at 400 rotations per minute (rpm) to amass electrospun fibers onto the PLA yarn. Nanoyarns with core-sheath structure were collected by the collecting roller rotating at 7 rpm. A total four strands of nanofiber yarns were combined into a singular strand and were knitted into scaffolds. PLLA/SF nanofiber yarns and knitted scaffolds were denoted as PS, while PLLA/SF nanofiber yarns and knitted scaffolds containing 2, 4, 8, 16 μg/mL of tetrandrine was denoted as PS-T2, PS-T4, PS-T8, and PS-T16, respectively.

2.4. Network pharmacology analysis

Target genes were identified using GeneCards, Therapeutic Target Database (TTD), and Y Mendelian Inheritance in Man (OMIM) databases with the keyword “soft tissue regeneration” and the structural formula of tetrandrine. The intersection of the potential targets was imported into Protein-Protein Interaction (PPI) Network Analysis, GO (Gene Ontology) Function, and KEGG (Kyoto Encyclopedia of Genes and Genomes) Enrichment Analysis. The GO enrichment analysis included biological process (BP), cell composition (CC), and molecular function (MF). The top 10 genes were chosen according to the number of involved targets ($p < 0.05$). On the other hand, KEGG pathway analysis was performed for the top 30 targets ($p < 0.05$) and was screened for the signal pathways with high enrichment.

2.5. Characterization of electrospun fibers and knitted scaffolds

2.5.1. Micromorphology

The micromorphology of yarns and knitted scaffolds was discerned by scanning electron microscopy (SEM, Phenom XL, Phenom Scientific, Netherlands). Samples were coated with the gold (current, 10 mA, 45 s) before visualization. The average diameter of fibers was measured by Image J software (National Institutes of Health, v1.8.0, USA) ($n = 100$).

2.5.2. Mechanical properties

The mechanical properties of yarns and knitted scaffolds were characterized by a universal material testing machine (Instron-5542, Canton, USA) at ambient temperature (*ca.* 25 °C) and humidity (*ca.* 55 %). A 200 N load cell (Transcell Technology, Inc., BAB- 20MT, USA) was used to stretch the samples at a strain rate of 20 mm/min. At least 5 samples were tested for each group. The ultimate tensile strength (UTS), strain at failure value, Young’s modulus, and failure force were calculated according to the stress-strain curves.

2.5.3. Water contact angle

The water contact angle of knitted scaffolds and PLLA micron fiber yarn was determined by a Dynamic contact angle analyzer (DCA322W, Thermo fisher, USA) and analyzed by Image J software.

2.5.4. FTIR assay

The structural analysis was carried out using Fourier Transform infrared spectroscopy (FTIR, AVATAR 380, Therm Electron, USA). Samples were analyzed in the range of 4000–400 cm^{-1}.

2.6. Biocompatibility and anti-inflammatory ability

2.6.1. Hemolysis assay

The hemocompatibility of knitted scaffolds was discerned by hemolysis assay. The fresh blood was collected from SD rats and centrifuged at 3000 rpm for 10 min to obtain the erythrocytes, which were then diluted to 2 % (v/v) suspension with SPSS. 1 mL of RBCs suspension was incubated along with the scaffolds (5 mm × 2 mm) in an Eppendorf (EP) tube for 2 h and was centrifuged at 3000 rpm for 10 min. The absorbance of the supernatant was measured at 540 nm using a microplate reader (Multiskan MK3, Thermo fisher, USA). Normal saline and DI water were used as negative and positive controls, respectively. The hemolysis ratio of the knitted scaffolds was calculated according to Eq. (1):

$$\text{Hemolysis ratio} = \frac{(A_T - A_N)}{(A_P - A_N)} \times 100\% \quad (1)$$

where A_T stands for the optical density (OD) of the knitted scaffolds, A_P and A_N represent the corresponding OD values of positive and negative control groups, respectively.

2.6.2. Cell culture

Tenocytes and NIH-3T3 fibroblasts were used as representative cell lines to evaluate the biocompatibility and anti-fibrotic ability of the knitted scaffolds. Tenocytes were cultured in α-MEM supplemented with 10 % fetal bovine serum, and 1 % Penicillin-Streptomycin solution. On the other hand, NIH-3T3 fibroblasts were cultured in 10 % FBS- and 1 % Penicillin-Streptomycin-supplemented DMEM. Cells were incubated at

37 °C, 5 % CO_2 in a humidified incubator and the culture medium was replaced every 2 d Meanwhile, knitted scaffolds (PS, PS-T4, PS-T8, and PS-T16) were immersed in culture medium for 24 h at 37 °C after Ultraviolet sterilization to obtain extract solution. Once cells achieved 80 % confluence, they were harvested using 0.25 % trypsin and were either seeded in a 48-well plate for live/dead staining or in a 24-well plate for migration and anti-inflammatory ability at a cell density of 20,000 per well. For cell adhesion, the cell-seeded plates were initially incubated for 24 h in the complete medium. Thereafter, the medium was replaced with the extract solution for different time points.

2.6.3. Cell proliferation assay and fluorescent staining

At day 1, 3, and 5, cell proliferation was studied with Cell Counting kit-8 (CCK-8) assay. The extract solution was aspirated and replaced either with DMEM (for NIH-3T3 fibroblasts) or α-MEM (for tenocytes) supplemented with 10 % CCK-8 solution. The plates were incubated at 37 °C for 2 h while being protected from the light. The optical density (OD) of the supernatant was measured at 450 nm using a microplate reader (Multiskan MK3, Thermo).

At day 5, the viability of the cells was evaluated using propidium iodide (PI, 0.5 μM) and Calcein AM (0.25 μM) (Calcein-AM/PI Kit). Cells were washed with phosphate buffered saline (PBS) two times to completely remove the extract solution and were stained with Calcein-AM/PI according to the manufacturer's introduction, and incubated at 37 °C for 20 min under light protection. An inverted fluorescent microscope (IX53, Olympus) was used to observe the morphology of the stained cells.

For cell cytoskeletal staining, samples were stained with Rhodamine phalloidin. Briefly, at day 5 after cell seeding, cells were washed with the PBS for two times, fixed using 4 % paraformaldehyde solution, and stained with Alexa Fluor@568 phalloidin (5 μg/mL) according to the manufacturer's instructions for 45 min. The cells were washed with PBS and stained with DAPI for 5 min and observed using the inverted fluorescence microscope. All experiments were run in triplicate.

2.6.4. Cell migration assay

The chemotactic ability of the scaffolds for tenocytes and NIH-3T3 fibroblasts was studied using a transwell migration assay. Cells (10,000) were seeded into inserts, while serum-free scaffold extract was placed into the wells and plates were incubated for 24 h. Subsequently, the cells that have migrated through the membrane were stained with crystal violet staining solution and observed using the inverted microscope.

A scratch wound healing assay was further performed for the tenocytes. Tenocytes were cultured in 24-well plates at a density of 1×10^4 cells/well and incubated at least for up to 8 h to allow cell adhesion. A scratch was made using a 200 μL pipette tip on the center of the wells. Cells were then incubated in serum-free scaffold extract for up to 12 h. Cell scratches were observed at 0, 12, and 24 h of incubation using the inverted microscope and wound area was calculated by Image J software. Each group (PS, PS-T4, PS-T8, and PS-T16) was run in quadruplicate.

2.6.5. Anti-inflammatory assay

To discern the anti-inflammatory ability of knitted scaffolds, tenocytes were co-cultured along with RAW264.7 macrophages. RAW264.7 macrophages were placed into inserts at a density of 1×10^4 cells/well, while tenocytes cultured along with the extract solution of scaffolds were placed in the wells and incubated for 24 h. Tenocytes were stained with F-actin/DAPI following manufacturer's instructions and incubated at 37 °C. The morphology of the cells was observed using an inverted fluorescence microscopy for the cell cytoskeleton.

2.7. Biocompatibility of scaffolds in vivo

To diserv the biocompatibility of the knitted scaffolds *in vivo*, a subcutaneous implantation model was used. SD rats were anesthetized by intraperitoneal injection of pentobarbital sodium (40 mg/kg) and the skin was shaved. An incision was made on the mid-line and subcutaneous pocket was created using forceps. The knitted scaffolds (2 mm × 5 mm) in PS, PS-T4, and PS-T8 group were implanted and the skin was sutured. Intramuscular injection of 1×10^4 units of penicillin was given once a day for 3 days ($n = 3$). The subcutaneously implanted scaffolds were harvested at week 4 and week 8 post-operatively. Samples were fixed in 10 % formalin solution for 48 h, dehydrated with a graded series of ethanol, paraffin-embedded and sectioned. Hematoxylin-eosin (H&E) and Masson's trichrome (MT) staining was performed.

2.8. Tendon repair effect of scaffolds in vivo

Patellar tendon defects in rats were used to evaluate the repair effect of the knitted scaffolds. SD rats were anesthetized using 3 % pentobarbital sodium (1 mL/kg) by intraperitoneal injection. A 3-cm incision was made on the medial of the knee to expose the patellar tendon. In the center of the patellar tendon, a full-thickness defect (2 mm × 20 mm) was made. The knitted scaffolds were cropped into strips (2 mm × 20 mm) and then sutured to the defective portion of the patellar tendon. The skin was sutured. Intramuscular injection of 4×10^5 units of penicillin was given once a day for 3 days. The repaired patellar tendon samples were explanted at week 6 post-operatively and were fixed in 10 % formalin solution for 48 h, dehydrated with a graded series of ethanol, paraffin-embedded and sectioned, H&E and MT staining was given subsequently.

2.9. Statistical analysis

All results are based on experiments conducted a minimum of three times, and expressed as mean ± standard deviation (SD). The statistical significance was analyzed by one-way analysis of variance (ANOVA) followed by Tukey's post hoc test. The significant difference was $^*p < 0.05$, $^{**}p < 0.01$, $^{***}p < 0.001$.

3. Result

3.1. Network pharmacology

The biological activity and potential mechanism between tetrandrine (Fig. 2a) and soft tissue regeneration were clarified by network pharmacology. Based on the Pubchem, SSTP, and CTD databases, 168 potential tetrandrine-related targets were identified after screening and reselection. Moreover, based on the GC, TTD, and OMIM databases, 3359 potential targets related to the soft tissue repair were obtained based. By considering the intersection of these results, 124 intersecting targets were identified between tetrandrine and soft tissue repair (Fig. 2b-d).

The GO enrichment analysis revealed that salient biological processes during soft tissue regeneration included protein phosphorylation, serine and tyrosine phosphorylation, cell apoptosis, cell proliferation, and intracellular signal transduction. Cellular components manifested the localization of targets mainly in cytosol, cytoplasm, membrane raft, nucleus, plasma membrane, caveola, and nucleoplasm. Moreover, according to the molecular function, these targets played a pivotal role in protein kinase activity, adenosine triphosphate (ATP) binding, protein serine/threonine kinase activity, identical protein binding, protein kinase binding, and so on (Fig. 2e). The Kyoto Encyclopedia of Genes and Genomes (KEGG) enrichment analysis showed that the common genes of tetrandrine were involved in different signaling pathways, such as advanced glycation end products (AGE)-receptor for advanced glycation end products (RAGE) signaling pathway and phosphatidylinositol 3-kinase (PI3K)-Akt signaling pathway (Fig. 2f). In terms of soft tissue repair, AGE-RAGE signaling pathway can lead to the expression of inflammatory genes and promote inflammation, while PI3K-Akt signaling

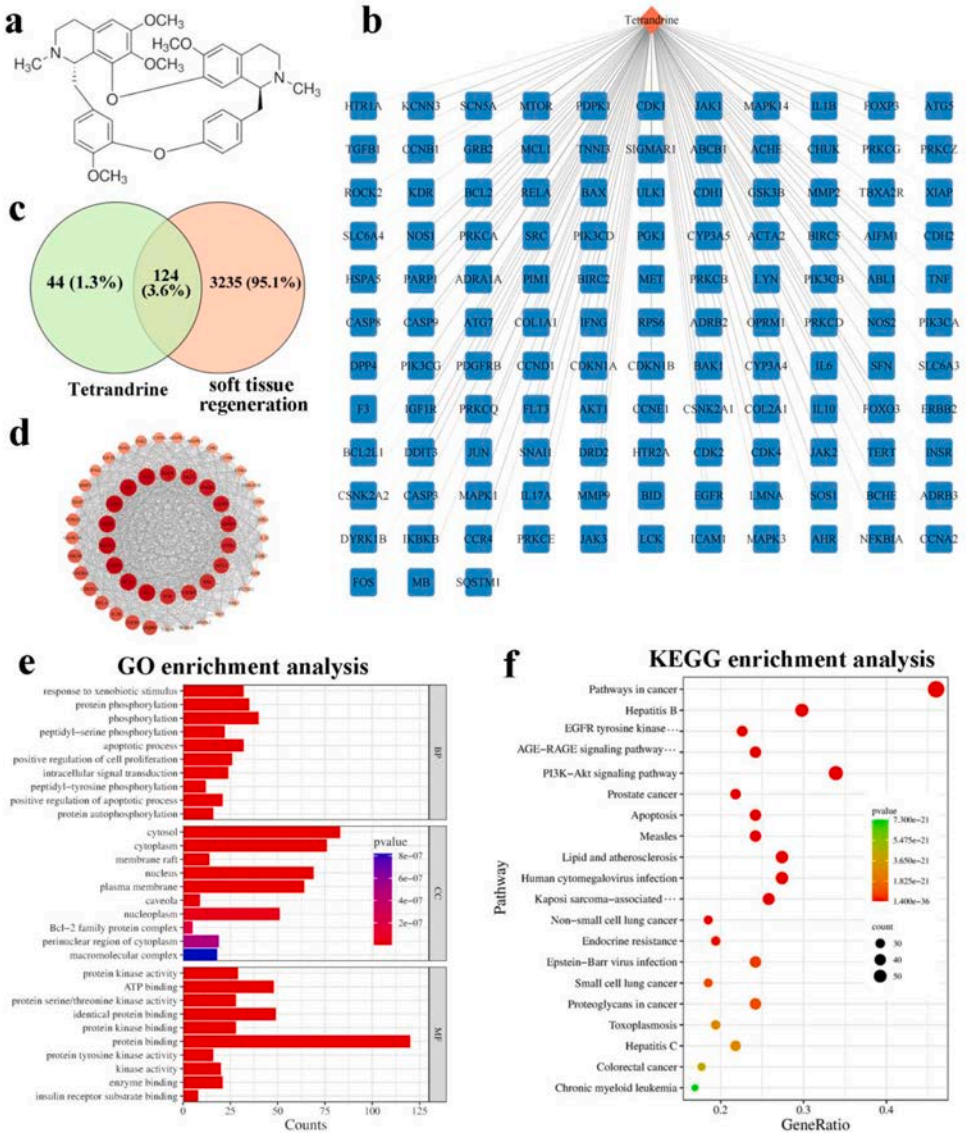

Fig. 2. Structural formula of tetrandrine (a). The network of the relationship between the tetrandrine and targets (b). Venn diagram of soft tissue regeneration targets with the targets of tetrandrine active components. (c). The PPI network of tetrandrine's targets for the treatment of soft tissue regeneration (d). The GO enrichment analysis of tetrandrine's therapeutic target (top 10 results of BP, CC, MF enrichment analysis respectively) (e). The KEGG enrichment analysis of tetrandrine's therapeutic targets (the top 30 results) (f).

pathway enhances glycolysis under hypoxia and promotes fibroblasts proliferation [34,35]. Aboval results indicated that tetrandrine could improve soft tissue repair through orchestrating multiple pathways.

3.2. *Characteristics of nanofiber yarns and knitted scaffolds*

Surface micro-morphology of tetrandrine-loaded nanoyarns and knitted scaffolds (PS, PS-T2, PS-T4, PS-T8, and PS-T16, named according to the concentration of tetrandrine) is shown in Fig. 3a. PLLA micron fiber yarns exhibited an oriented structure and served as a core layer with nanofibers randomly wrapped around the core. The average diameters of fibers were found to be 0.55 ± 0.13 μm, 0.55 ± 0.15 μm, 0.54 ± 0.16 μm, 0.50 ± 0.13 μm and 0.53 ± 0.19 μm on the surface of PS, PS-T2, PS-T4, PS-T8, and PS-T16, respectively. Structural analysis of nanoyarns was carried out using FTIR. The band appearing at 1750 cm^{-1} is ascribed to the ester groups of the PLLA, while the band at 1655 cm^{-1} is ascribed to the amide bond of the SF. The PS group manifested bands ascribed to the ester group and the amide bond. The tetrandrine-loaded nanoyarns manifested an additional characteristic peak at 685 cm^{-1}, which is attributed to the benzene ring in tetrandrine as observed in PS-T4 and PS-T16 (Fig. 3b).

Hydrophilicity of nanoyarns with or without the incorporation of the drug was evaluated by measuring the water contact angle (WCA). The WCA of nanoyarns was significantly decreased with an increase in the drug content (WCA values: PS-T16, 36.3 ± 0.4°; PS-T8, 53.0 ± 0.1°; PS-T4, 59.1 ± 2.2°, PS-T2, 87.2 ± 0.5°; and PS, 99.2 ± 2.7°), indicating an increase in the hydrophilicity with an increase in the tetrandrine content in the scaffolds, which could provide a better environment for cell adhesion and proliferation (Fig. 3c).

To ascertain the mechanical properties of nanofiber-coated PLLA micron fiber yarns as well as knitted scaffolds, uniaxial tensile testing was performed. The representative stress-strain curves manifested linear elasticity in the initial region while plastic deformation beyond the yield point as the stress was further increased (Fig. 3d, i). For nanoyarns, UTS of PS, PS-T2, PS-T4, PS-T8, and PS-T16 was significantly higher than that of the PLLA micron fiber yarns albeit similar elongation at break (Eb) values. These results showed that the electrospun fibers increased the UTS of yarns. While there was an insignificant difference among

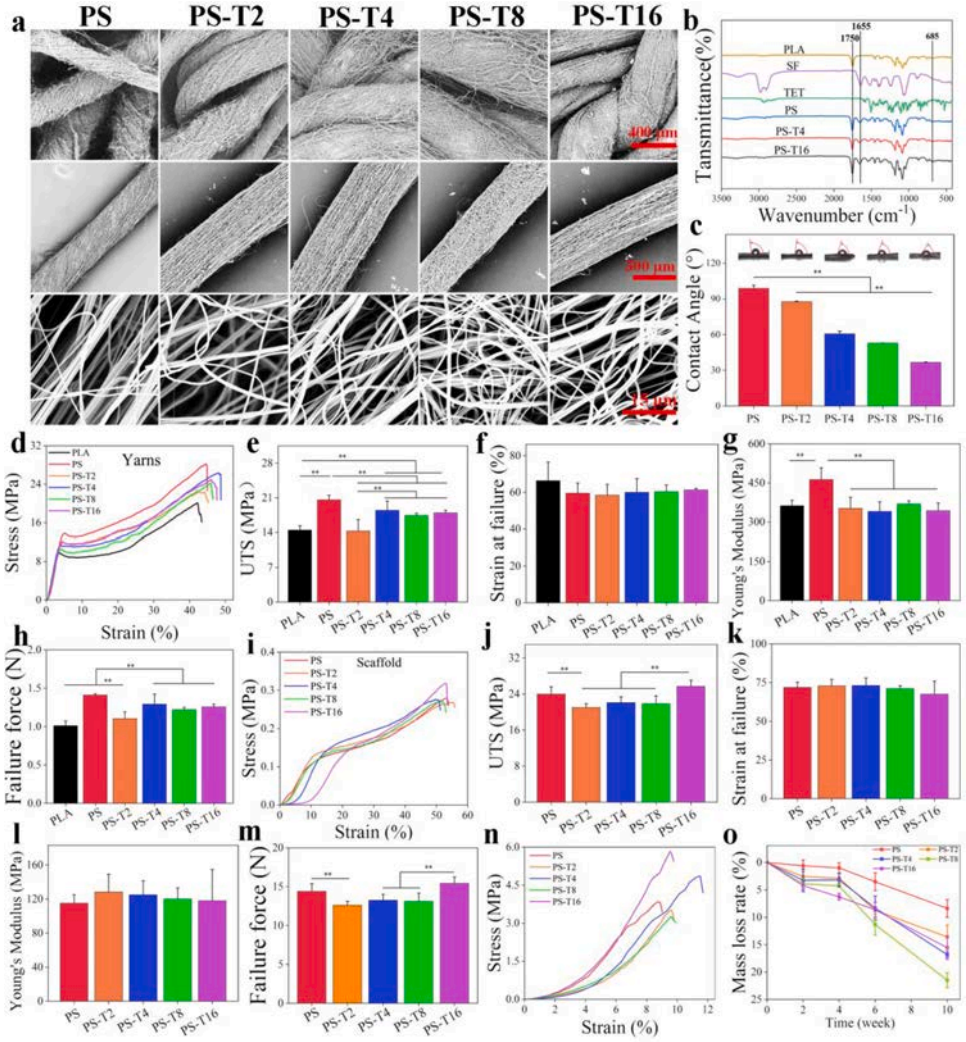

Fig. 3. SEM images of knitted scaffolds and yarns (a). FTIR spectra of the PLA, SF, TET, PS, PS-T4, and PS-T16 samples (b). The water contact angle of knitted scaffolds (c). Representative tensile stress-strain curves (d), UTS (e), Eb (f), Young's modulus (g), and failure force (h) of nanofiber yarns. Representative tensile stress-strain curves (i), UTS (j), Eb (k), Young's modulus (l), and failure force (m) of knitted scaffolds. Representative tensile stress-strain curves of knitted scaffolds after 10 weeks of degradation (n). The mass loss rate after knitted scaffolds degradation (o). * $p < 0.05$, ** $p < 0.01$ ($n = 5$).

various drug-loaded nanoyarns (*e.g.*, PS-T2, PS-T4, PS-T8, PS-T16, etc.) in terms of the UTS, the UTS and Young's modulus of these drug-loaded nanoyarns were significantly less as compared to the PS group with negligible difference in the Eb values (Fig. 3e-h). The reduction in the UTS of the fibers-coated PLLA micron fiber yarns upon drug loading can be ascribed to the drug.

On the other hand, knitted scaffolds exhibited lower Young's modulus while higher Eb and UTS value than that of the nanoyarns, which is indicative of the better elasticity of the knitted scaffolds. Besides, knitted scaffolds exhibited significantly higher failure force than that of the nanofibers-coated yarns (failure force: knitted scaffolds, 13.8 ± 1.3 N and yarns, 1.22 ± 0.14 N). It is worthy to note that the UTS and Young's modulus of human natural tendon tissue are 5–100 MPa and 20–1200 MPa, respectively [36]. The corresponding values of the knitted scaffolds are within the range of the UTS and *E* of the human tendinous tissues (Fig. 3j-m).

The degradation of the knitted scaffolds was further discerned *in vitro*. After 10 weeks of degradation in aseptic PBS, the strain-stress curves of knitted scaffolds did not show plastic deformation beyond the yield point, which is suggestive of an increased rigidity of scaffolds (Fig. 3n). Moreover, knitted scaffolds manifested an increase in the degradation with an increase in the tetrandrine content, possibly due to increased hydrophilicity, which is consistent with the result of WCA above. Consistent with clinical demands, knitted scaffolds maintain integrity during early repair stage (<4 weeks) and then gradually degrade to transfer biomechanical loads to regenerated tissue [6,37]. The PS-T8 group exhibited the highest average mass loss rate (21.5 ± 1.4 %) at week 10 (Fig. 3o).

3.3. Cell viability and cell morphology

The cytocompatibility of nanoyarns as well as knitted scaffolds was discerned by using two distinct cell types namely: tenocytes and NIH-3T3 fibroblasts. Both cell types largely remained alive with only a few numbers of dead cells for up to day 5. While the number of alive NIH-3T3 fibroblasts were gradually decreased with an increase in the concentration of tetrandrine, the number of tenocytes were increased with an increase in the drug content (Fig. 4a). The cells cultured along with the conditioned medium of different types of scaffolds were further subjected to the cytoskeletal staining for the F-actin with Alexa Fluor@568 phalloidin. The NIH-3T3 fibroblasts manifested a spindle-like morphology. On the other hand, tenocytes displayed a fusiform-like morphology (Fig. 4b).

The cell proliferation was also studied by a CCK-8 assay. The

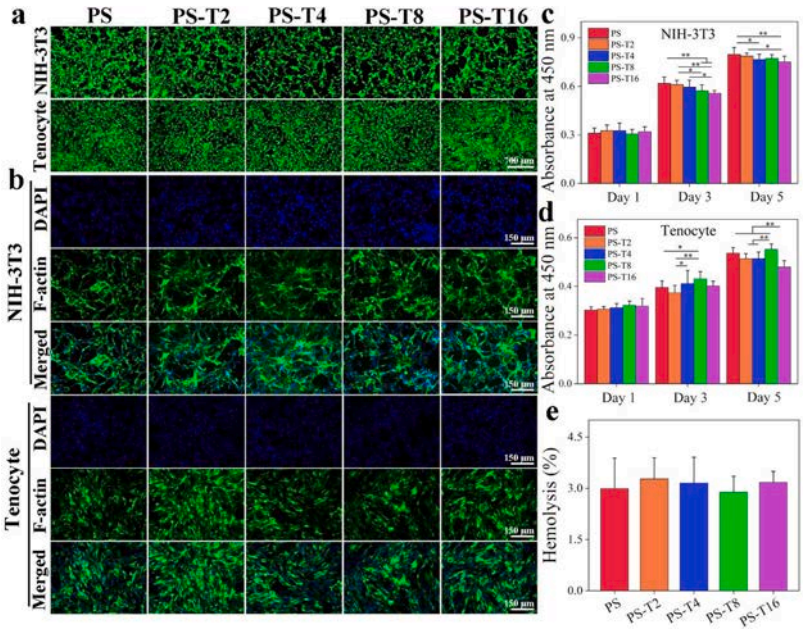

Fig. 4. The cytocompatibility of tenocytes and NIH-3T3 fibroblasts cultured along with the extract solution obtained from different types of knitted scaffolds. Live (green) / dead (red) staining (a) and DAPI (blue)/F-actin (green) staining (b) of tenocytes and NIH-3T3 fibroblasts cultured in the scaffolds' extract as observed at day 5. Scale bar = 700 μm and scale bar = 150 μm. The proliferation of NIH-3T3 fibroblasts (c) and tenocytes (d) was as elucidated using CCK-8 assay. The blood compatibility of knitted scaffolds (e). * $p < 0.05$, ** $p < 0.01$ ($n = 3$).

tenocytes showed gradual proliferation from day 1 to day 5 albeit an insignificant difference among various groups (*e.g.*, PS, PS-T4, PS-T8, PS-T16, etc.) as earlier as day 1. On the other hand, PS-T8 outperformed PS in terms of the growth of the tenocytes both at day 3 and 5. It is worthy to note that the PS-T16 displayed less cell proliferation than that of the other groups both at day 3 and 5, drug-induced cytotoxicity at higher concentrations.

The proliferation of the NIH-3T3 fibroblasts was decreased with an increase in the tetrandrine content, which is suggestive of the inhibitory effect of the drug on the cell proliferation (Fig. 4d). Taken together, these results indicated the beneficial effect of the tetrandrine on the viability and growth of the tenocytes with an optimal drug dose of 8 μg/mL with negligible cytotoxicity yet significant cell proliferation over the times (Fig. 4c).

Since in most of the cases, the implanted biomaterials directly contact the blood after implantation *in vivo*, we further delineated

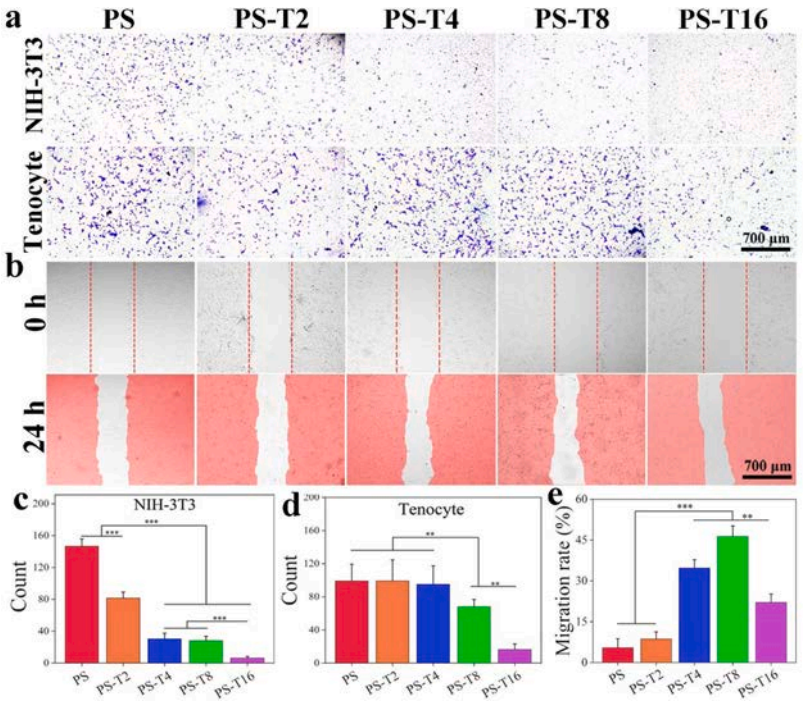

Fig. 5. Cell migration activity. Crystal violet staining of NIH-3T3 fibroblasts and tenocytes on the lower side of the transwell inserts as delineated using an inverted microscope (a, c, d). Images of tenocytes in scratch wound healing assay at initial, 12 h and 24 h (b) and the wound area calculated using Image J software (e). *$p < 0.05$, **$p < 0.01$, *** $p < 0.001$ ($n = 3$).

hemolysis. The results revealed hemolysis rate of less than 5 % both for the nanoyarns and the knitted scaffolds, which is indicative of their good hemocompatibility and is within the ISO standards (Fig. 4e).

3.4. Cell migration

A transwell migration assay was carried out to determine cell migration activity *in vitro*, which mirrored the live/dead staining and CCK-8 assay. The number of NIH-3T3 fibroblasts migrated towards the lower side of the transwell inserts were appreciably decreased with an increase in the drug content in the scaffolds (PS, 146.7 ± 9.1 cells/HPF; PS-T2, 81.5 ± 7.6 cells/HPF; PS-T4, 30.3 ± 7.6 cells/HPF). In the PS-T16 group, NIH-3T3 was barely visible (6.2 ± 2.2 cells/HPF). In contrast, sufficiently higher number of tenocytes with good morphology were observed on the lower surface of the inserts in the PS, PS-T2, PS-T4, and PS-T8 groups albeit drastic reduction in the number of tenocytes in the PS-T16 group (Fig. 5a, c, d).

The scratch wounding assay was further performed using tenocytes and the images were quantified by image J software. The scratch area was decreased over time (Fig. 5b). By 24 h, the scratch area was significantly lower in the PS-T16 group than that of the PS group, which is indicative of the beneficial effect of tetrandrine on the migration of tenocytes (Fig. 5e).

3.5. Anti-inflammatory and anti-adhesion effect of scaffolds

To discern anti-inflammatory effect of tetrandrine, the expression of different macrophage markers was evaluated by flow cytometry (Fig. 6a). The CD206/CD68 ratio was considerably increased with an increase in the tetrandrine content (Fig. 6b-d), which is ascribed to the ability of the drug to promote the macrophages polarization towards M2 phenotype and may also have implications for the anti-inflammatory properties of scaffolds.

The tenocytes were also co-cultured with RAW264.7 macrophages for up to 24 h, which exhibited quadrilateral shape alongside a spread morphology. On the other hand, tenocytes were reversed to their original fusiform-like morphology with the incorporation of tetrandrine (Fig. 6e). The quantification with image J also manifested significantly higher aspect ratio of tenocytes cultured alongside the extract solution of the PS-T4 (4.70 ± 0.83) than that of the PS (1.54 ± 0.26) and PS-T2 (2.31 ± 0.66) groups. Taken together, these data indicated the anti-inflammatory effect of knitted scaffold with an optimal dose of tetrandrine for up to 4 μg/mL (Fig. 6f).

3.6. Biocompatibility of scaffolds in vivo

Based on the promising results *in vitro*, the biocompatibility of PS-T4 and PS-T8 was further assessed *in vivo*. The knitted scaffolds were implanted in SD rats for up to 8 weeks (Fig. 7a). The H&E and MT staining displayed gradual infiltration of host cells as well as deposition of collagen at the interface of the host tissues and scaffolds, which was further increased with an increase in the implantation time. The PS-T8 group exhibited higher number of recruited cells and collagenous tissues than that of the PS and PS-T4 groups (Fig. 7b-c). These results showed that the knitted scaffolds can degrade and allow the infiltration of host cells as well as the deposition of collagen.

3.7. Tendon repair in vivo

The regenerative effect of the knitted scaffolds was further elucidated in a rat patellar tendon defects model *in vivo* (Fig. 8a). Models with implantation of knitted scaffolds in PS-T4 and PS-T8 groups showed similar macroscopic view to the normal group, while defects in PS group and control group showed obvious inflammation (Fig.8b). The H&E staining exhibited knitted scaffolds alongside neotissues. The tendon defects treated with the PS, PS-T4, and PS-T8 manifested an accumulation of different types of cells (fibroblasts, inflammatory cells, red blood cells, etc.) alongside *de novo* blood vessels. The clearance area of

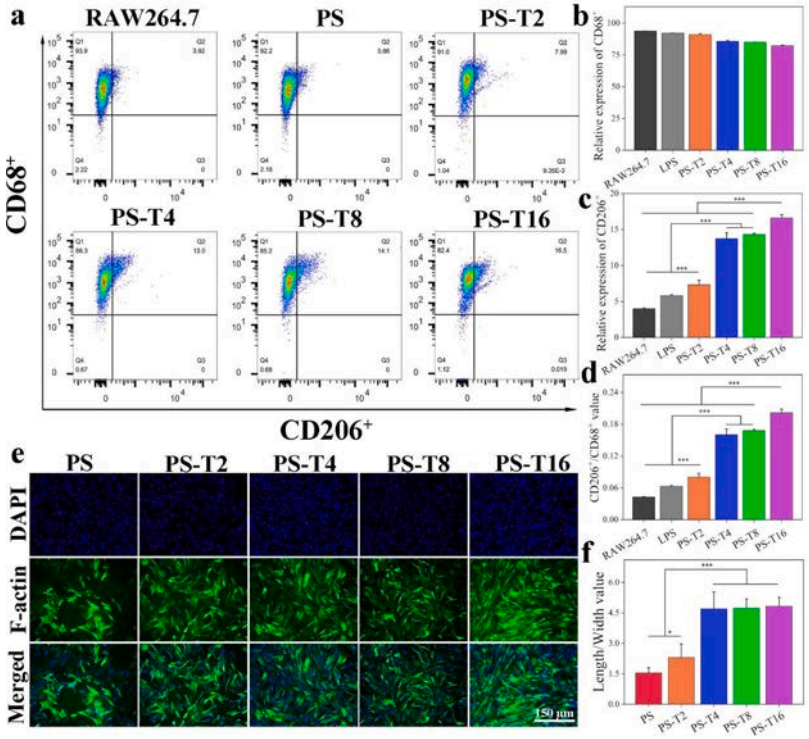

Fig. 6. Anti-inflammatory ability of tetrandrine: The macrophage markers CD206 / CD68 (a-d) were analyzed by flow cytometery. DAPI (blue)/F-actin (green) staining of tenocytes co-cultured along with RAW264.7 macrophages for 24 h and observed using an inverted fluorescent microscope (e), and the length / width value of tenocytes (f), scale bar = 150 μm. *$p < 0.05$, **$p < 0.01$, *** $p < 0.001$ ($n = 3$).

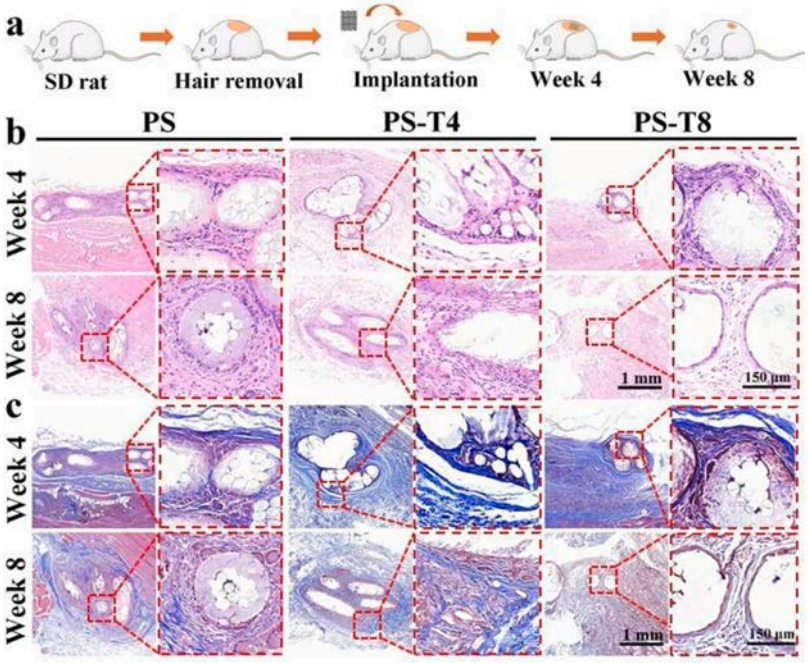

Fig. 7. Biocompatibility of knitted scaffolds. Schematic illustration of subcutaneous embedding test (a). Macroscopic view of H&E staining of embedded site on week 4 and week 8 (b). Macroscopic view of MT staining of embedded site on week 4 and week 8 (c), scale bar = 1 mm, and scale bar = 150 μm.

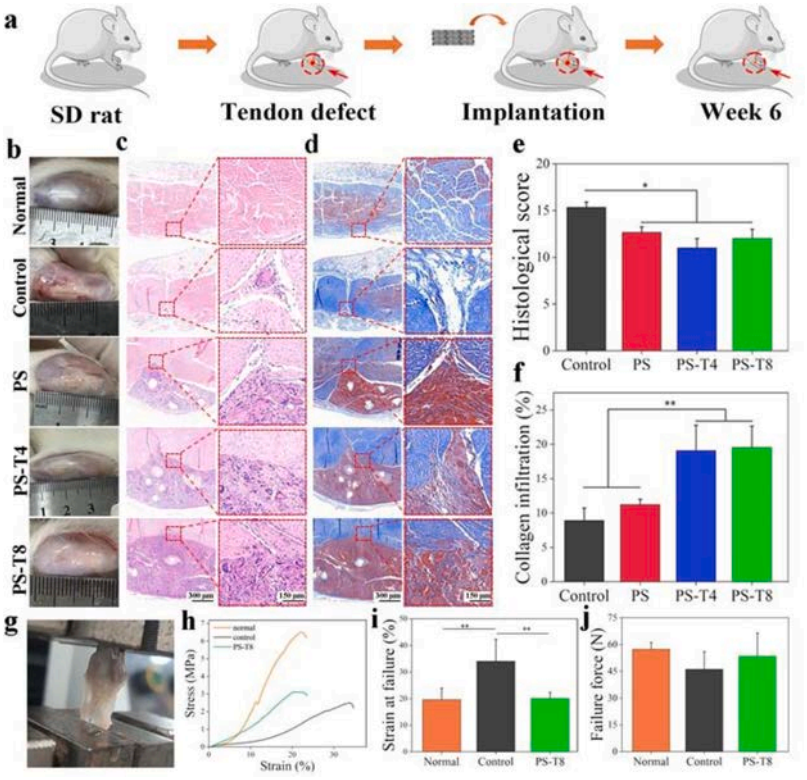

Fig. 8. Tendon reconstruction with the implantation of knitted scaffolds in a patellar tendon model *in vivo*. Schematic illustration of the implantation of knitted scaffolds at the defective portion of rat's patellar tendon (a). Macroscopic view of knitted scaffold in tendon repair (b), H&E staining (c), MT staining (d), histological score (e), and collagen infiltration (f). The image after tendon strain (g). The stress-strain curve (h), Eb (i) and failure force (j) of tendons after 6 weeks. scale bar = 300 μm, and scale bar = 150 μm. Normal: native tendon. Control: defective untreated tendons. * $p < 0.05$, ** $p < 0.01$. ($n = 4$).

tissue-scaffold interface was significantly reduced in the PS group than that of the control group (defects devoid of any treatment); the PS-T4 and PS-T8 outperformed the PS and control groups in terms of the clearance area reduction. The adhesion between the knitted scaffolds and tendon was considerably increased with the incorporation of drug, which is indicative of the beneficial effect of knitted scaffolds for the tendon repair (Fig.8c & e). Masson's trichrome staining further showed significantly higher collagen deposition at the defect site in the PS-T4

and PS-T8 groups than that of the PS group, which is further suggestive of the regenerative effect of knitted scaffolds on tendon repair (Fig.8d & f). The results of mechanical tests for tendons indicated that although the mechanical properties of PS-T8 group have not yet fully reached the level of normal tendons, it still exhibited a superior recovery compared to the control groups. This suggests that the treatment applied in the PS-T8 group is effective in enhancing the mechanical strength and functionality of the tendon repair process (Fig.8g-j). Semi-Quantitative Histopathological Scoring was based on previous reports [38].

4. Discussion

Peritendinous adhesion is a common complication of joint dysfunction and is as an undesirable outcome of the tendon healing process [39]. In this study, we developed a novel knitted scaffold which exhibited good mechanical properties, anti-inflammatory, and anti-fibrotic characteristics. Unlike conventional approaches that rely on separate pharmacological agents, tetrandrine provided simultaneous anti-inflammatory and anti-fibrotic regulation, which is a critical advancement over current monofunctional therapies. PLLA micron fiber yarns were coated with electrospun tetrandrine-loaded PLLA/SF nanofibers, which were then processed into knitted scaffolds. Mechanical properties of the knitted scaffolds were better than that of the PLLA/SF-coated nanoyarns and therefore these knitted scaffolds may be more suitable for tendon repair (Fig. 3d-m). Tetrandrine-loaded knitted scaffold suppressed overproliferation of NIH-3T3 fibroblasts as well as regulated macrophages polarization from an inflammatory M1 phenotype into anti-inflammatory M2 phenotypes. Since an excessive proliferation of myofibroblasts and prolonged inflammatory response are linked to the fibrosis, anti-inflammatory and anti-fibrotic characteristics of the scaffolds may have implications for the treatment of peritendinous adhesions. Indeed, we leveraged these knitted scaffolds for a rat tendon adhesion model, wherein PS-T4 group (tetrandrine concentration: 4 μg/ml) outperformed the other groups in terms of the inhibition of tissue adhesion and scar tissue formation, and neotissue formation (Fig. 8).

Inflammation is an integral part of the healing process immediately after tendon injury [40]. During an initial inflammatory stage, macrophages accumulate at the site of an injured tissue and coordinate various healing processes. Nevertheless, an excessive accumulation of pro-inflammatory M1 macrophages may adversely affect the tendon repair, which necessitates the advent of the strategies to regulate the proliferation of macrophages as well as regulation of the inflammatory response for a healthier yet effective tissue repair. The PS-T4 group manifested anti-inflammatory characteristics as revealed by the flow cytometry assay and the co-culture of the tenocytes along with the RAW264.7 macrophages (Fig. 6). Tetrandrine-loaded knitted scaffolds reduced the production of the pro-inflammatory cytokines secreted by the RAW264.7 macrophages. It is worthy to note that these pro-inflammatory factors secreted from stimulated macrophages, such as cyclooxygenase-2 (COX-2) and interleukin-6 (IL-6) may affect the morphology of the tenocytes, thereby altering them from a fusiform-like morphology to flat quadrilateral-like morphology [41], while PS-T4 scaffolds restored tenocytes to their original shape.

In tendon regeneration, the inflammatory stage is followed by the proliferative stage, in which mesenchymal stem cells (MSCs) and fibroblasts from different sources are involved in an earlier repair of tendons [42]. Unlike tenocytes, which proliferate slowly, fibroblasts from the surrounding tissues migrate and invade into the injured tissues, rapidly proliferate, and differentiate into myofibroblasts [43]. Nevertheless, overproliferation of fibroblasts may cause tissue adhesion and limit the ability of the tendon to slide in flexion alongside rendering the neotendon tissue mechanically fragile and prone to the repeat ruptures. Consequently, it is imperative to suppress an over proliferation of fibroblast for a healthier and functional tendon repair. Among all studied groups, the PS-T4 not only inhibited migration and proliferation of NIH-3T3 fibroblasts but also enhanced the preferential migration and growth of tenocytes. Therefore, the tetrandrine-loaded scaffolds may offer a promising platform to balance the proliferation of tenocytes and myofibroblasts (Fig.5a).

Subcutaneous implantation of scaffolds in rats also showed good biocompatibility *in vivo* (Fig. 7). Similarly, transplantation of knitted scaffolds in a rat model constricted the clearance area at the scaffold-tissue interface alongside increased collagen deposition. It is worthy to notice that although PS-T4 (tetrandrine concentration: 4 μg/ml) and PS-T8 (tetrandrine concentration: 8 μg/ml) groups displayed similar anti-inflammatory effects *in vitro*, the former exhibited minimal inflammation than that of the PS-T8 group *in vivo* (Fig. 8). To put together, the knitted PS-T4 scaffolds may be beneficial in balancing inflammation and promoting, as well as playing an important role in long-term tendon repair.

However, the current study still has also some limitations. Firstly, the scaffolds were manually woven which may not be conducive, especially, compared to the automated woven scaffolds. Similarly, the knitted scaffolds manifested mechanical proprieties inferior to that of the normal tendons, which also requires further optimization. Secondly, while most experiments were repeated in triplicate ($n = 3$), a subset of critical validations employed higher replication ($n = 4$–5). Future studies would benefit from expanded sample sizes to enhance statistical robustness. Besides, while we have enhanced objectivity through semi-quantitative pathological scoring (Fig. 8e) and statistical analysis of collagen construction (Fig. 8f), the lack of complementary quantitative molecular data (*e.g.*, PCR or western blot) limits mechanistic interpretation of the observed phenotypic changes. Future studies will prioritize systematic preservation of samples for multi-omics integration, enabling correlation of structural improvements with molecular pathways.

5. Conclusions

In this study, a knitted scaffold with good mechanical, anti-inflammatory, and anti-fibrotic properties was successfully prepared by combining electrospinning and manual weaving. The incorporation of tetrandrine allowed the scaffolds to actively regulate the inflammatory response and inhibit excessive fibroblast proliferation, which are common challenges in tendon healing. PLLA micron fiber yarns were coated with electrospun tetrandrine-loaded PLLA/SF nanofibers, which were then weaved to afford the knitted scaffolds. The PS-T4 scaffold inhibited the excessive proliferation of fibroblasts, attenuated the inflammatory response as well as tissue adhesion, and had no significant toxicity to tendon cells. *In vivo* study, the PS-T4 demonstrated the ability to promote collagen regeneration and reduce inflammation and adhesion. Taken together, our approach of simultaneously harnessing structural and biological cues in the form of an antiproliferative and anti-inflammatory therapeutic alongside PLLA/SF-coated nanoyarns afforded knitted scaffolds, which may have broad implications for tendon tissue repair and potentially other related disciplines.

CRediT authorship contribution statement

Xinyan Chen: Writing – review & editing, Writing – original draft, Investigation, Funding acquisition, Formal analysis, Data curation, Conceptualization. **Xiao Yu:** Formal analysis, Data curation, Conceptualization. **Hao Feng:** Funding acquisition, Formal analysis. **Panpan Shang:** Supervision, Methodology, Conceptualization. **Muhammad Shafiq:** Writing – review & editing, Writing – original draft. **Zhengchao Yuan:** Data curation, Conceptualization. **Cheng Li:** Visualization. **Zewen Wang:** Validation. **Zhenchao Liu:** Validation. **Yuan Yao:** Validation. **Mohamed EL-Newehy:** Writing – review & editing. **Meera Moydeen Abdulhameed:** Writing – review & editing. **Yan Xiong:** Writing – review & editing. **Yuan Xu:** Writing – review & editing. **Xiumei Mo:** Funding acquisition, Conceptualization.

Declaration of competing interest

The authors declare that they have no known competing financial interests or personal relationships that could have appeared to influence the work reported in this paper.

Acknowledgments

This project was supported by the Fundamental Research Funds for the Central Universities (CUSF-DH-T-2023063), the Science and Technology Research Program of Chongqing Municipal Education Commission (KJZD-K202412807), Youth Doctoral Talent Incubation Program of the Second Affiliated Hospital, Army Medical University (2023YQB002), Science and Technology Commission of Shanghai Municipality, China (20DZ2254900), Sino German Science Foundation Research Exchange Center, China (M-0263), the Chenguang Program of Shanghai Education Development Foundation and Shanghai Municipal Education Commission (23CGB08), and China Education Association for International Exchange (2022181). This project was also supported by Researchers Supporting Project Number (RSP2025R65), King Saud University, Riyadh, Saudi Arabia

Data availability

Data will be made available on request.

References

[1] H. Aslan, N. Kimelman-Bleich, G. Pelled, D. Gazit, Molecular targets for tendon neoformation, J. Clin. Invest. 118 (2008) 439–444, https://doi.org/10.1172/JCI33944.
[2] D. Docheva, S.A. Müller, M. Majewski, C.H. Evans, Biologics for tendon repair, Adv. Drug Deliv. Rev. 84 (2015) 222–239, https://doi.org/10.1016/j.addr.2014.11.015.
[3] X. Yu, Y. Shen, J. Cui, Y. Ding, Y. Morsi, B. Sun, X. Mo, H. Gu, The potential application of electrical stimulation in tendon repair : a review, Med-X (2025). 10.1007/s44258-025-00051-9.
[4] J. Zhang, C. Xiao, X. Zhang, Y. Lin, H. Yang, Y.S. Zhang, J. Ding, An oxidative stress-responsive electrospun polyester membrane capable of releasing antibacterial and anti-inflammatory agents for postoperative anti-adhesion, J. Control Release 335 (2021) 359–368, https://doi.org/10.1016/j.jconrel.2021.04.017.
[5] H.G. Jørgensen, S.D. McLellan, J.F. Crossan, A.S.G. Curtis, Neutralisation of TGFβ or binding of VLA-4 to fibronectin prevents rat tendon adhesion following transection, Cytokine 30 (2005) 195–202, https://doi.org/10.1016/j.cyto.2004.12.017.
[6] P.B. Voleti, M.R. Buckley, L.J. Soslowsky, Tendon healing: repair and regeneration, M.L. Yarmush (Ed.), Annu. Rev. Biomed. Eng. 14 (2012) 47–71, https://doi.org/10.1146/annurev-bioeng-071811-150122. VOL.
[7] A. Hoffmann, G. Gross, Tendon and ligament engineering: from cell biology to *in vivo* application, Regen. Med. 1 (2006) 563–574.
[8] D.A. Oakes, D.R. McAllister, Failure of heat shrinkage for treatment of a posterior cruciate ligament tear, Arthroscopy 19 (2003) e1–e4.
[9] L. Li, X. Zheng, D. Fan, S. Yu, D. Wu, C. Fan, W. Cui, H. Ruan, Release of celecoxib from a bi-layer biomimetic tendon sheath to prevent tissue adhesion, Mater. Sci. Eng. C 61 (2016) 220–226, https://doi.org/10.1016/j.msec.2015.12.028.
[10] X. Xie, J. Cai, Y. Yao, Y. Chen, A. ur R. Khan, J. Wu, X. Mo, A woven scaffold with continuous mineral gradients for tendon-to-bone tissue engineering, Compos. Part B Eng. 212 (2021) 108679, https://doi.org/10.1016/j.compositesb.2021.108679.
[11] C. Cai, X. Zhang, Y. Li, X. Liu, S. Wang, M. Lu, X. Yan, L. Deng, S. Liu, F. Wang, C. Fan, Self-healing hydrogel embodied with macrophage- regulation and responsive-gene-silencing properties for synergistic prevention of peritendinous adhesion, 2106564 (2022) 1–12. 10.1002/adma.202106564.
[12] X. Yu, J. Cui, Y. Shen, W. Guo, P. Cai, Y. Chen, Z. Yuan, M. Liu, M. EL-Newehy, H. EL-Hamshary, Y. Morsi, B. Sun, M. Shafiq, X. Mo, Current advancements and strategies of biomaterials for tendon repair: a review, FBL 28 (2023) 66–null.
[13] Y. Chen, M. Shafiq, M. Liu, Y. Morsi, X. Mo, Advanced fabrication for electrospun three-dimensional nanofiber aerogels and scaffolds, Bioact. Mater. 5 (2020) 963–979, https://doi.org/10.1016/j.bioactmat.2020.06.023.
[14] Z. Yan, X. Meng, Y. Su, Y. Chen, L. Zhang, J. Xiao, Double layer composite membrane for preventing tendon adhesion and promoting tendon healing, Mater. Sci. Eng. C 123 (2021) 111941, https://doi.org/10.1016/j.msec.2021.111941.
[15] A. Sensini, C. Gotti, J. Belcari, A. Zucchelli, M.L. Focarete, C. Gualandi, I. Todaro, A.P. Kao, G. Tozzi, L. Cristofolini, Morphologically bioinspired hierarchical nylon 6,6 electrospun assembly recreating the structure and performance of tendons and ligaments, Med. Eng. Phys. 71 (2019) 79–90, https://doi.org/10.1016/j.medengphy.2019.06.019.
[16] M. EI, Healing of subcutaneous tendons: influence of the mechanical environment at the suture line on the healing process., (2025).
[17] L. Gil-Melgosa, J. Grasa, A. Urbiola, R. Llombart, M. Susaeta Ruiz, V. Montiel, C. Ederra, B. Calvo, M. Ariz, P. Ripalda-Cemborain, F. Prosper, C. Ortiz-de-Solórzano, J. Pons-Villanueva, A. Pérez Ruiz, Muscular and tendon degeneration after achilles rupture: new insights into future repair strategies, Biomedicines 10 (2021), https://doi.org/10.3390/biomedicines10010019.
[18] X. Yu, G. Shen, J. Yan, W. Guo, Z. Yuan, J. Cui, Y. Shen, P. Cai, Y. Chen, M. Tsz, M. El-newehy, Induction of macrophage polarization by electrospun nano-yarn containing naproxen sodium to promote tendon repair, Appl. Mater. Today 36 (2024) 102070, https://doi.org/10.1016/j.apmt.2024.102070.
[19] G. Walden, X. Liao, S. Donell, M.J. Raxworthy, G.P. Riley, A. Saeed, A clinical, biological, and biomaterials perspective into tendon injuries and regeneration, Tissue Eng. Part B Rev. 23 (2016) 44–58, https://doi.org/10.1089/ten.teb.2016.0181.
[20] F. Wu, M. Nerlich, D. Docheva, General orthopaedics Tendon injuries : basic science and new repair proposals, 2 (2017). 10.1302/2058-5241.2.160075.
[21] S. Dooley, B. Delvoux, M. Streckert, L. Bonzel, M. Stopa, P. ten Dijke, A. M. Gressner, Transforming growth factor β signal transduction in hepatic stellate cells via Smad2/3 phosphorylation, a pathway that is abrogated during *in vitro* progression to myofibroblasts: tGFβ signal transduction during transdifferentiation of hepatic stellate cel, FEBS Lett. 502 (2001) 4–10, https://doi.org/10.1016/S0014-5793(01)02656-4.
[22] Y. Chen, D. Li, J. Wu, Y. Chen, H. Lu, Tetrandrine inhibits activation of rat hepatic stellate cells stimulated by transforming growth factor-β *in vitro* via up-regulation of Smad 7, J. Ethnopharmacol. 100 (2005) 299–305, https://doi.org/10.1016/j.jep.2005.03.027.
[23] Z. Zhang, X.J. Li, Y. Liu, X. Zhang, Y.Y. Li, W.S. Xu, Recombinant human decorin inhibits cell proliferation and downregulates TGF-β1 production in hypertrophic scar fibroblasts, Burns 33 (2007) 634–641, https://doi.org/10.1016/j.burns.2006.08.018.
[24] Y. Xi, H.J. Zhang, Z.G. Ye, G.P. Zhang, Research development on modern pharmacological effect of tetrandrine, Zhongguo Zhongyao Zazhi 45 (2020) 20–28, https://doi.org/10.19540/j.cnki.cjcmm.20190830.401.
[25] L. Zunwen, L. Shizhen Z FAU - Dewu, M. Dewu L FAU - Yungui, N. Yungui M FAU - Pu, N. Pu, Effect of tetrandrine on the TGF-β-induced smad signal transduction pathway in human hypertrophic scar fibroblasts *in vitro*. PG - 404-13 LID, 10.1016/j.burns.2011.08.013 [doi], (2025).
[26] L.N. Gao, Q.S. Feng, X.F. Zhang, Q.S. Wang, Y.L. Cui, Tetrandrine suppresses articular inflammatory response by inhibiting pro-inflammatory factors via NF-κB inactivation, J. Orthop. Res. 34 (2016) 1557–1568, https://doi.org/10.1002/jor.23155.
[27] T. Chen, X. Zhao, Y. Weng, Self-assembled polylactic acid (PLA): synthesis, properties and biomedical applications, (2023) 1–8. 10.3389/fchem.2022.1107620.
[28] F. Imani, R. Karimi-Soflou, I. Shabani, A. Karkhaneh, PLA electrospun nanofibers modified with polypyrrole-grafted gelatin as bioactive electroconductive scaffold, Polymer 218 (2021) 123487, https://doi.org/10.1016/j.polymer.2021.123487 (Guildf).
[29] Z. Cai, X. Mo, K. Zhang, L. Fan, A. Yin, Fabrication of chitosan /silk fibroin composite nanofibers for wound-dressing applications, (2010) 3529–3539. 10.3390/ijms11093529.
[30] W. Sun, D.A. Gregory, M.A. Tomeh, X. Zhao, Silk fibroin as a functional biomaterial for tissue engineering, (2021) 1–28.
[31] S. Jiang, X. Zhao, S. Chen, G. Pan, J. Song, N. He, F. Li, W. Cui, C. Fan, Down-regulating ERK1/2 and SMAD2/3 phosphorylation by physical barrier of celecoxib-loaded electrospun fibrous membranes prevents tendon adhesions, Biomaterials 35 (2014) 9920–9929, https://doi.org/10.1016/j.biomaterials.2014.08.028.
[32] X. Liu, X. He, D. Jin, S. Wu, H. Wang, M. Yin, A. Aldalbahi, M. El-Newehy, X. Mo, J. Wu, A biodegradable multifunctional nanofibrous membrane for periodontal tissue regeneration, Acta Biomater. 108 (2020) 207–222, https://doi.org/10.1016/j.actbio.2020.03.044.
[33] L. Wei, S. Wu, M. Kuss, X. Jiang, R. Sun, P. Reid, X. Qin, B. Duan, 3D printing of silk fibroin-based hybrid scaffold treated with platelet rich plasma for bone tissue engineering, Bioact. Mater. 4 (2019) 256–260, https://doi.org/10.1016/j.bioactmat.2019.09.001.
[34] S. Sukjamnong, H. Chen, S. Saad, R. Santiyanont, Fimbristylis ovata and Artemisia vulgaris extracts inhibited AGE-mediated RAGE expression, ROS generation, and inflammation in THP-1 cells, Toxicol. Res. 38 (2022) 331–343, https://doi.org/10.1007/s43188-021-00114-0.
[35] Q.F. Wang, X. Yang, J.X. Ma, X. Xie, Y.M. Sun, X. Chang, H.S. Bi, H.Y. Xue, Z.L. Qin, PI3K/AKT pathway promotes keloid fibroblasts proliferation by enhancing glycolysis under hypoxia, Wound Repair Regen. 31 (2023) 139–155, https://doi.org/10.1111/wrr.13067.
[36] A.S. LaCroix, S.E. Duenwald-Kuehl, R.S. Lakes, R. Vanderby, Relationship between tendon stiffness and failure: a metaanalysis, J. Appl. Physiol. 115 (2013) 43–51, https://doi.org/10.1152/japplphysiol.01449.2012.
[37] R. Li, Performance and dynamical characteristics of three-dimensional stent materials in tendon tissue engineering, J. Clin. Rehabil. Tissue Eng. Res. 14 (2010) 1447–1450, https://doi.org/10.3969/j.issn.1673-8225.2010.08.028.
[38] M. Loppini, U.G. Longo, G. Niccoli, W.S. Khan, N. Maffulli, V. Denaro, Histopathological scores for tissue-engineered, repaired and degenerated tendon: a systematic review of the literature, Curr. Stem Cell Res. Ther. 10 (2015) 43–55, https://doi.org/10.2174/1574888X09666140710110723.
[39] Y. Li, C. Hu, B. Hu, J. Tian, G. Zhao, C. Cai, Y. Li, Z. Sun, S. Wang, S. Pang, R. Bao, Z. Tao, H. Chen, J. Wu, S. Liu, Sustained release of dicumarol via novel grafted

polymer in electrospun nanofiber membrane for treatment of peritendinous adhesion, Adv. Healthc. Mater. 12 (2023) 1–12, https://doi.org/10.1002/adhm.202203078.
[40] N.L. Leong, J.L. Kator, T.L. Clemens, A. James, Tendon and ligament healing and current approaches to tendon and ligament regeneration, (2020) 7–12. 10.1002/jor.24475.
[41] C.T. Thorpe, S. Chaudhry, I.I. Lei, A. Varone, G.P. Riley, H.L. Birch, P.D. Clegg, H. R.C. Screen, Tendon overload results in alterations in cell shape and increased markers of inflammation and matrix degradation, Scand. J. Med. Sci. Sports 25 (2015) e381–e391, https://doi.org/10.1111/sms.12333.
[42] K.B. Sugg, J. Lubardic, J.P. Gumucio, C.L. Mendias, Changes in macrophage phenotype and induction of epithelial-to-mesenchymal transition genes following acute Achilles tenotomy and repair, J. Orthop. Res. 32 (2014) 944–951, https://doi.org/10.1002/jor.22624.
[43] J. Hou, R. Yang, I. Vuong, F. Li, J. Kong, H.Q. Mao, Biomaterials strategies to balance inflammation and tenogenesis for tendon repair, Acta Biomater. 130 (2021) 1–16, https://doi.org/10.1016/j.actbio.2021.05.043.